

Battery-Free Neuromodulator for Peripheral Nerve Direct Stimulation

Sanghoon Lee,^{‡1,2,3,4,6} Hao Wang,^{‡1,3,4,6} Jiahui Wang,^{1,2,6} Qiongfeng Shi,^{1,3,4,6} Shih-Cheng Yen,^{1,2}, Nitish V. Thakor,^{1,2,5,6} and Chengkuo Lee^{*1,2,3,4,5,6}

¹Department of Electrical and Computer Engineering, National University of Singapore, Singapore 117583, ²Singapore Institute for Neurotechnology (SINAPSE), National University of Singapore, Singapore 117456, ³Center for Intelligent Sensors and MEMS, National University of Singapore, Singapore 117576, ⁴NUS Suzhou Research Institute (NUSRI), Suzhou, Industrial Park, Suzhou, P. R. China 215123, ⁵Graduate School for Integrative Science and Engineering, National University of Singapore, Singapore 117456, ⁶Hybrid Integrated Flexible Electronic Systems (HiFES), National University of Singapore, Singapore 117608

‡Both authors contributed equally, E-mail: elelc@nus.edu.sg

Supporting Information

Contents

Section S1. Fabrication process of the WATENG	2
Section S2. Analysis of the enhancement of WATENG	4
Section S3. Detailed structure of the hydrogel based device	6
Section S4. Rat preparation for <i>in vivo</i> test	7
Section S5. Physiological Characterization and statistical analysis.....	8
Section S6. Electrochemical characterization of neural interface.....	9
Section S7. The peak-to-peak amplitude of the CMAPs from 3 pairs of neural electrode	11
Section S8. Force recording system	14
Reference.....	15

Section S1. Fabrication process of the WATENG

The detailed fabrication process of the WATENG array is illustrated in Fig. S1. Fig. S1-a1 to S1-a4 shows the process of the top and bottom PDMS films with ITO/PET electrodes. A reservoir with pin array made by 3D printing is used to pattern the PDMS films (Fig. S1-a1). The the reservoir is filled with PDMS (Fig. S1-a2) and then cure and release it off from the mold (Fig. S1-a3). There will be an array of holes on the PDMS film which can be used for further assembly. An array of ITO/PET electrodes is attached onto the PDMS film and fixed by double sided tape (Fig. S1-a4). Then, the 5 layers are assembled together to form the WATENG. The PDMS films with ITO/PET electrodes are used as the top and bottom electrodes. The top and bottom PDMS films are aligned and fixed with the spacer 1 and spacer 2, respectively. There is pin array on the two spacers which can be aligned and inserted into the hole array on the PDMS films. On the bottom surface of the spacer 1, there is an array of protruding structure which can be aligned and inserted into the array concave structure on the top surface of the spacer 2. These protruding and concave structure is used to clamp and fix the thin PDMS film and meanwhile make the thin PDMS film stretched, providing the recovery force required for the operation of WATENG. The detailed dimension illustration is shown in Fig. S1-d.

(a1): Mold by 3D printing



(a2): Fill the mold by PDMS



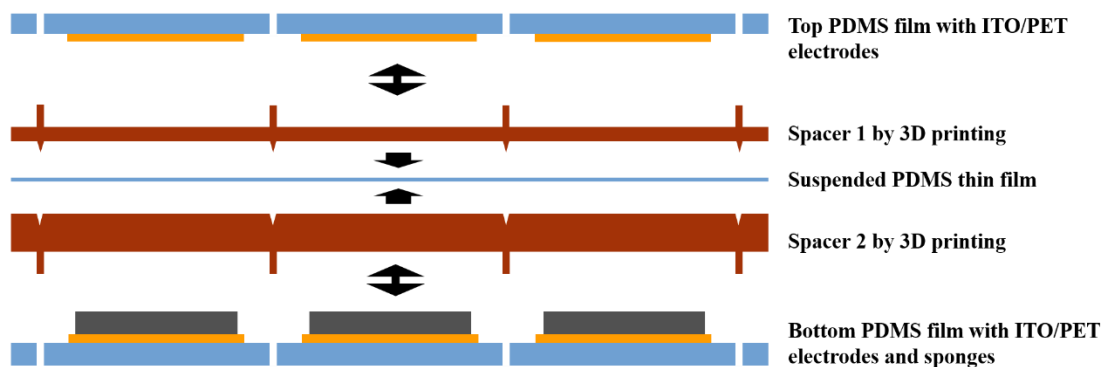
(a3): release the PDMS off from the mold



(a4): Attach the ITO/PET film onto the PDMS film



(b) Assemble 5 layers together



(c) Assembled WATENG

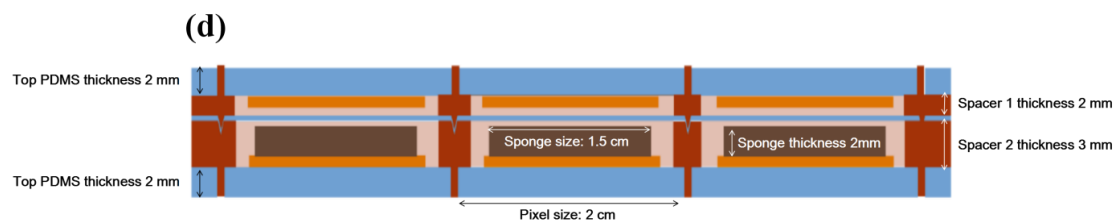
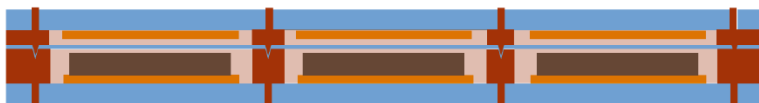


Figure S 1. Fabrication process and dimension illustration of the WATENG

Section S2. Analysis of the enhancement of WATENG

To confirm that lifting up the suspended thin film can enhance the output, three different structures were tested. For the case 1 in Fig. S2a, the dielectric thin film, which is the PDMS thin film here, is attached onto the electrode surface. This structure is widely adopted in previous studies of liquid involved TENGs [1-5]. For the structure in case 2 (Fig. S2b), the height of the spacer 2 is lower than the thickness of the sponge. After assembly of the whole device, the PDMS thin film was already fully stretched by the protruding top surface of the sponge and cannot be lifted up when the top thick PDMS recovered after being pressed. Meanwhile, the sponge filled with water was partially compressed, making the top surface contacting the PDMS thin film wetted. The case 3 (Fig. S2c) is the structure we developed which enable the suspended thin film to be lifted up. Normally the output of case 1 is at mV scale when the load resistance is lower than 1 M Ω . Due to the low inner impedance previously mentioned, the output will be lower than the noise level when high load resistance is applied. Thus, to make a fair comparison, all the tests of these three structures were conducted with 1 M Ω load resistance.

The testing results of these three structures are shown in Fig. S2d. The voltage of case 1 is lower than 10 mV which is consistent with the amplitude of minor peaks in Fig. 2c of the main text. The voltage of case 2 mainly is induced by the contact electrification between the top surface of the thin PDMS film and the top ITO surface. Due to the high inner impedance, the voltage output is also higher. However, the bottom surface of the PDMS thin film is always contact with the wet surface, meaning the negative charges on the bottom surface of the PDMS thin film is always balanced by the water in sponge. Hence during the pressing the releasing procedure, the positive charges on the ITO is only affected by the negative charges on single side of the PDMS thin film, making the output voltage of case 2 lower than that of case 3, which the positive charges on ITO was affected by the negative charges on both sides of the PDMS thin film.

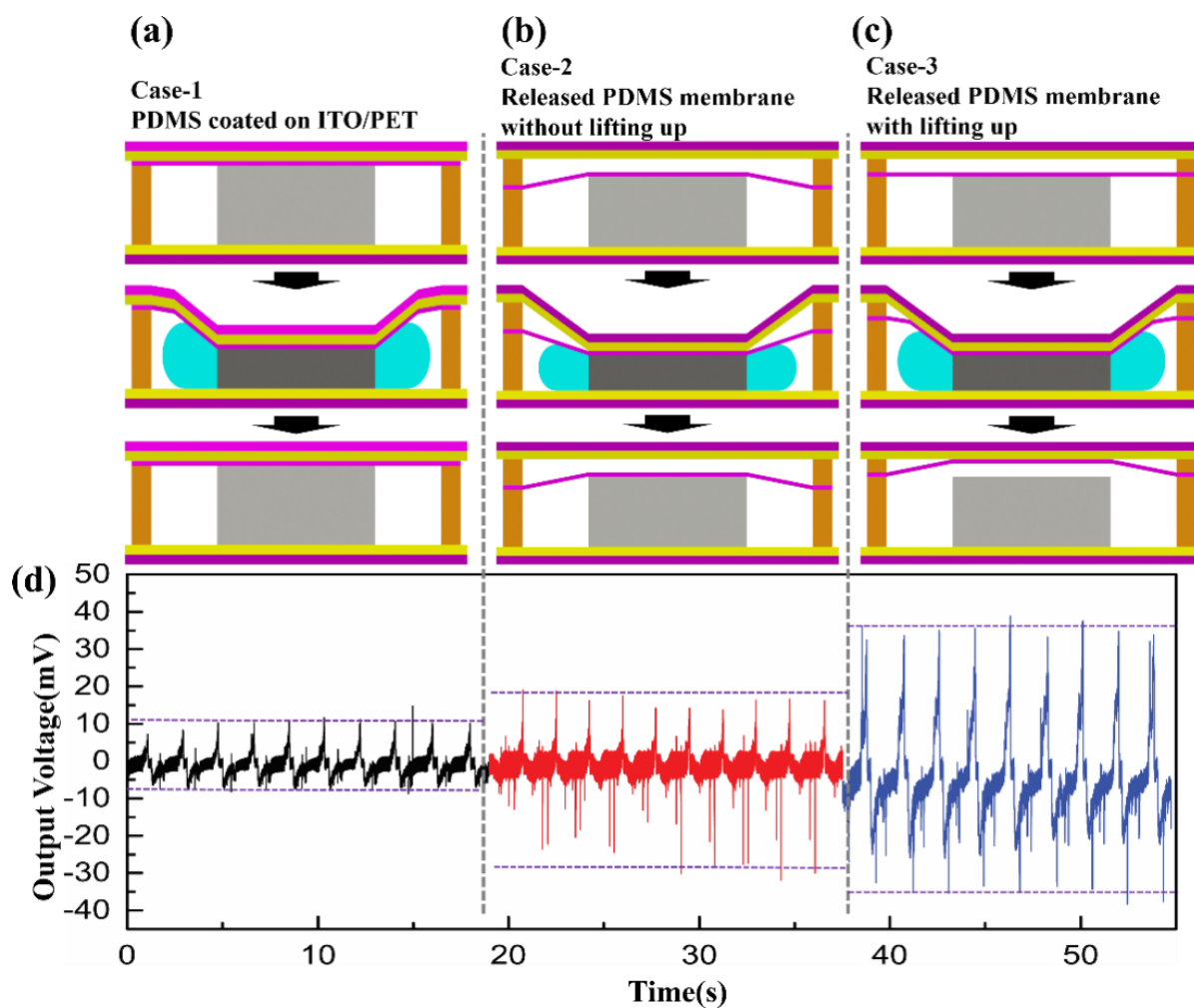
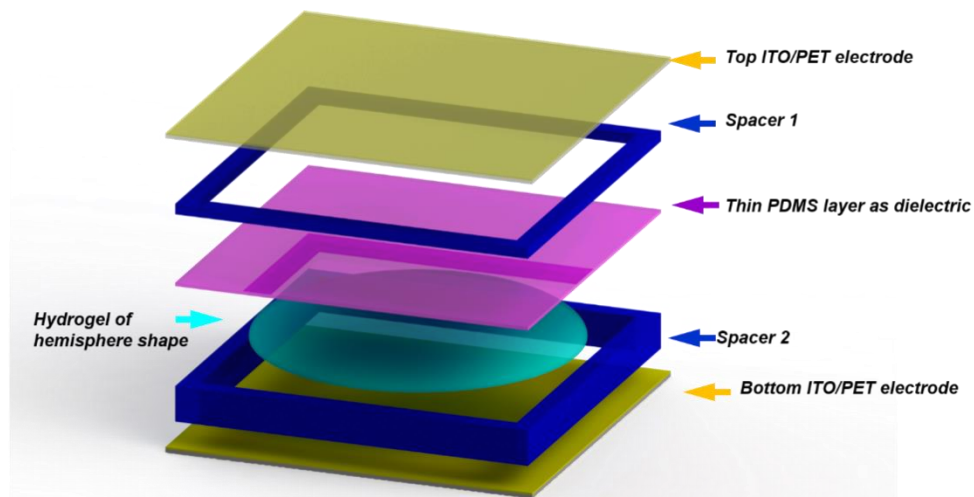


Figure S 2. Comparison of three different structures showing that lifting up the suspended thin film and enhance the output. (a) The conventional structure with thin film attached onto the electrode. (b) The thin film is suspended without lifting up. (c) The thin film is suspended and can be lifted up. (d) The voltage output of three structures when 1M Ω load was applied.

Section S3. Detailed structure of the hydrogel-based device

(a)



(b)

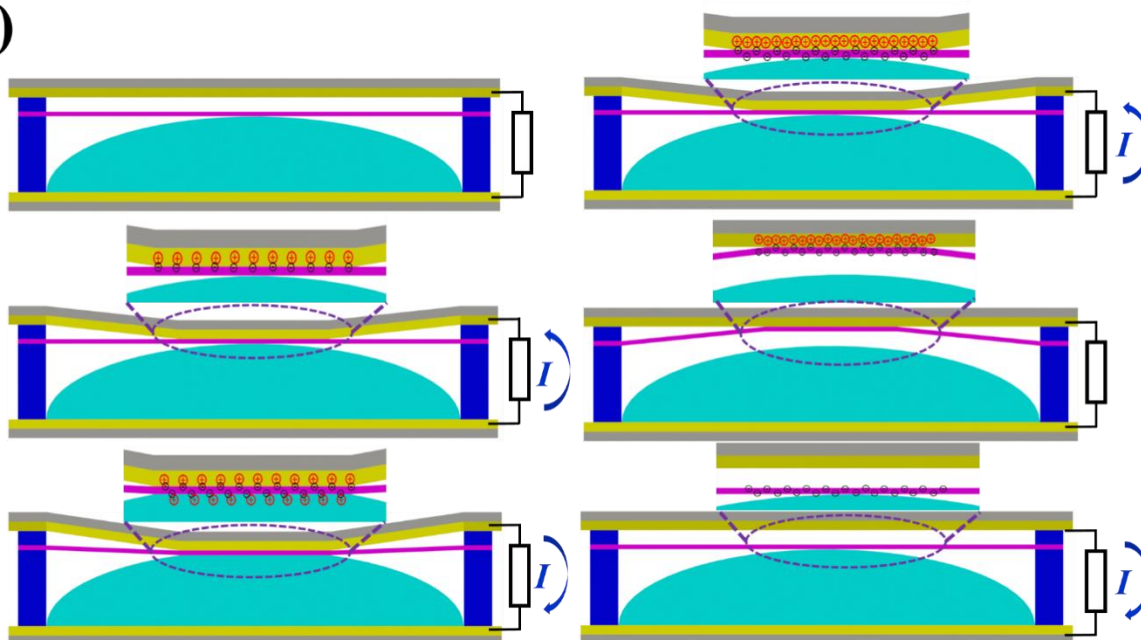


Figure S 3. Detailed structure and working principle of hydrogel-based device

Section S4. Rat preparation for *in vivo* test

The experiments were performed in adult female Sprague Dawley rats (250 g) (InVivos Pte Ltd, Singapore). The rats were acclimatized for one week prior to use in the experiment, with food and water provided ad libitum and 12 hour lights on/off. The animal care and use procedures were approved by those outlined by the Agri-Food & Veterinary Authority of Singapore (AVA), the Institutional Animal Care and Use Committee (IACUC), and the ethics commission of the National University of Singapore. The methods were carried out in accordance with 143/12 protocol. The animals were anesthetized with a single bolus injection of ketamine/xylazine (150 mg kg⁻¹ and 10 mg kg⁻¹, respectively, intraperitoneal). After an adequate depth of anesthesia was attained, the right sciatic nerves were exposed through a gluteal-splitting incision. Then, the sling electrodes were implanted on the sciatic nerves for the selecti stimulation. For the second *in vivo* experiment, a pair of Pt/Ir wires (A-M Systems, WA, USA) was implanted on the common peroneal (CP) nerve and the tibial nerve, respectively, to demonstrate the direct WATENG stimulation for the activation of leg muscles. The final *in vivo* experiment for the comparison of waveforms, a flexible neural clip (FNC) interface was implanted on the common peroneal (CP) nerve and the tibial nerve, respectively. The different waveforms (exponential peaks and pulsed waves) from a commercial stimulator (S48 Stimulator, Natus Medical Inc.) applied to the nerves, respectively, via FNC. Special care was taken to prevent nerve damage.

Section S5. Physiological Characterization and statistical analysis

For selective recording experiments, compound neural action potentials (CNAPs) from the main sciatic nerve were recorded using RHD2132 evaluation system (Intan Technologies). The sampling rate was 30 kHz and the muscles signals were filtered between 300 Hz and 3 kHz. The bipolar loop-hook electrodes were used for the CMAP recordings. A stainless steel needle inserted in the base of the tail was used as ground. Electrophysiological data were analyzed using custom-written algorithms in Matlab (Mathworks, Inc. USA). The CMAPs were identified after the stimulus artifact. The mean CMAPs were obtained from over 50 trials with intervals of 1 second between trials.

Section S6. Electrochemical characterization of neural interface

Electrochemical Characteristic Measurement

Electrochemical impedance spectroscopy (EIS) and cyclic voltammetry (CV) were performed to measure electrochemical characterization of the neural interfaces, respectively. The conventional three-electrode configuration was used. The sling electrode was used as a working electrode (WE) while a silver/silver chloride (Ag/AgCl) and a Pt wire gauze electrode were used as the reference (RE) and counter electrode (CE), respectively, in phosphate buffered saline (PBS). Impedance measurement was performed in a frequency range of 0.5 Hz – 30 kHz with a sinusoidal wave with amplitude of 10 mV. The output impedance was recorded with an impedance analyzer (Zennium E, ZAHNER-elektrik Inc, Germany). Water window from -0.6 V to 0.8 V, which is normal for Pt-black, was chosen with the sweep rate of 50 mV s⁻¹ for the CV test. The output CV was also recorded with cyclic voltammetry function in the impedance analyzer. The charge storage capacity (CSC) was calculated by the integration of area of CV plot and cathodic charge storage capacity (CSCc) was calculated by the integration of negative area (gray area in Fig. S4d) of the CV plot. The mean impedance of the Pt-black electrode was 2.3 kΩ at 1 kHz, which was 12 times lower than Au electrodes (Fig. S4b). The phase angle of the Pt electrodes at 1 kHz was -4.9° (Fig. S4c). It shows a small capacitive phase angle at low frequencies, which indicates capacitive impedance. The mean charge storage capacity (CSC) was 26.9 mC·cm⁻². Also, the mean cathodic charge storage capacity (CSCc) was 16.3 mC·cm⁻², indicated by the cathodic area of the CV plot (Fig. S4d). These values are comparable to materials used previously in the literature for neural stimulation [1-3]. As shown in Fig. S4d, the CV plot shows typical peaks for Pt-black, which indicates electrochemical reactions occurring at the electrode-electrolyte interface [4-6]. These results demonstrate that the Pt-black coated electrodes can be used for *in vivo* recording and stimulation experiments.

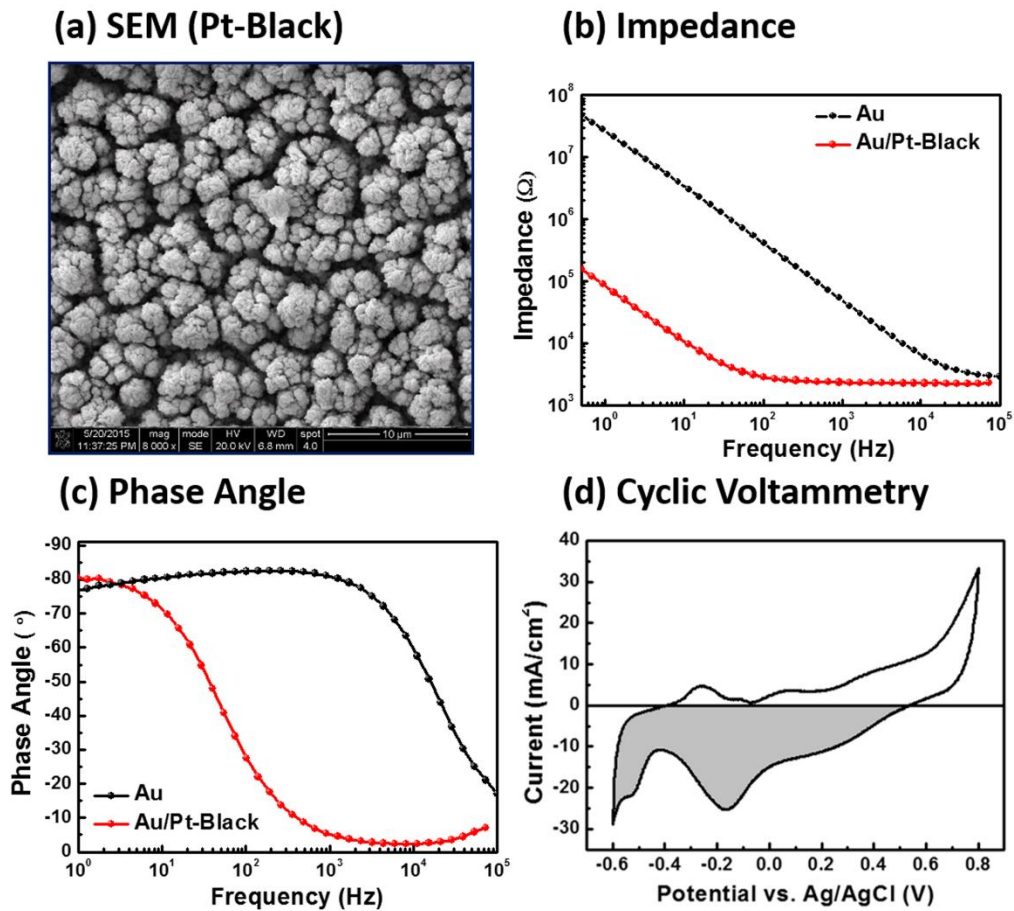


Figure S 4. (a) SEM image of Pt-black coated electrode. The results of EIS of Au and Pt-black for (b) impedance and (c) phase angle. (d) CV plot of Pt-black coated flexible and adjustable sling electrode.

Section S7. The peak-to-peak amplitude of the CMAPs from 3 pairs of neural electrode

The peak-to-peak amplitude of the CMAPs of 3 pairs of neural electrodes is shown in Figure S5. For the pair-1 which is close to the tibial nerve, the CMAPs of GM and TA is $5000 \mu\text{V} \pm 477 \mu\text{V}$ and $570 \mu\text{V} \pm 356 \mu\text{V}$ ($n=14$), respectively. For the pair-2 which is closer to the CP nerve, the CMAPs of GM and TA is $2700 \mu\text{V} \pm 513 \mu\text{V}$ and $2100 \mu\text{V} \pm 487 \mu\text{V}$ ($n=31$), respectively. For the pair-3, the CMAPs of GM and TA is $3200 \mu\text{V} \pm 674 \mu\text{V}$ and $830 \mu\text{V} \pm 213 \mu\text{V}$ ($n=63$), respectively.

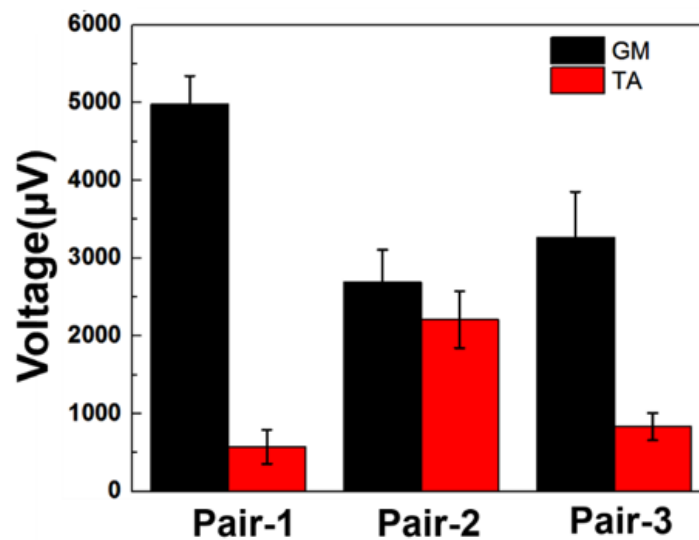


Figure S 5. The peak-to-peak amplitudes of the CMAPs from 3 pairs of neural electrodes

For the test of neural branch stimulation, we applied different force to press the WATENG. The charge for small force is around 1.5 nC (**Fig. S6a**) and for large force is 4 nC (**Fig. S6b**). The charge per phase was around 4 nC per phase. When we considered actual charge density applied to a nerve, 1.04 and 2.78 $\mu\text{C} \cdot \text{phase}^{-1} \cdot \text{cm}^{-2}$ were applied by the small force and the large forces, respectively. The threshold charge per phase of sciatic branches in rats was slightly less than human's ones [7-8]. The current for small force is 0.2 μA to 0.4 μA (**Fig. S6c**) and for large force is 0.4 μA to 0.6 μA (**Fig. S6d**). Because the force applied by hand tapping was not very stable as shown in (**Fig. S6e and f**). The small force is in the range from 3 N to 5 N and large force is in the range from 12 N to 19 N.

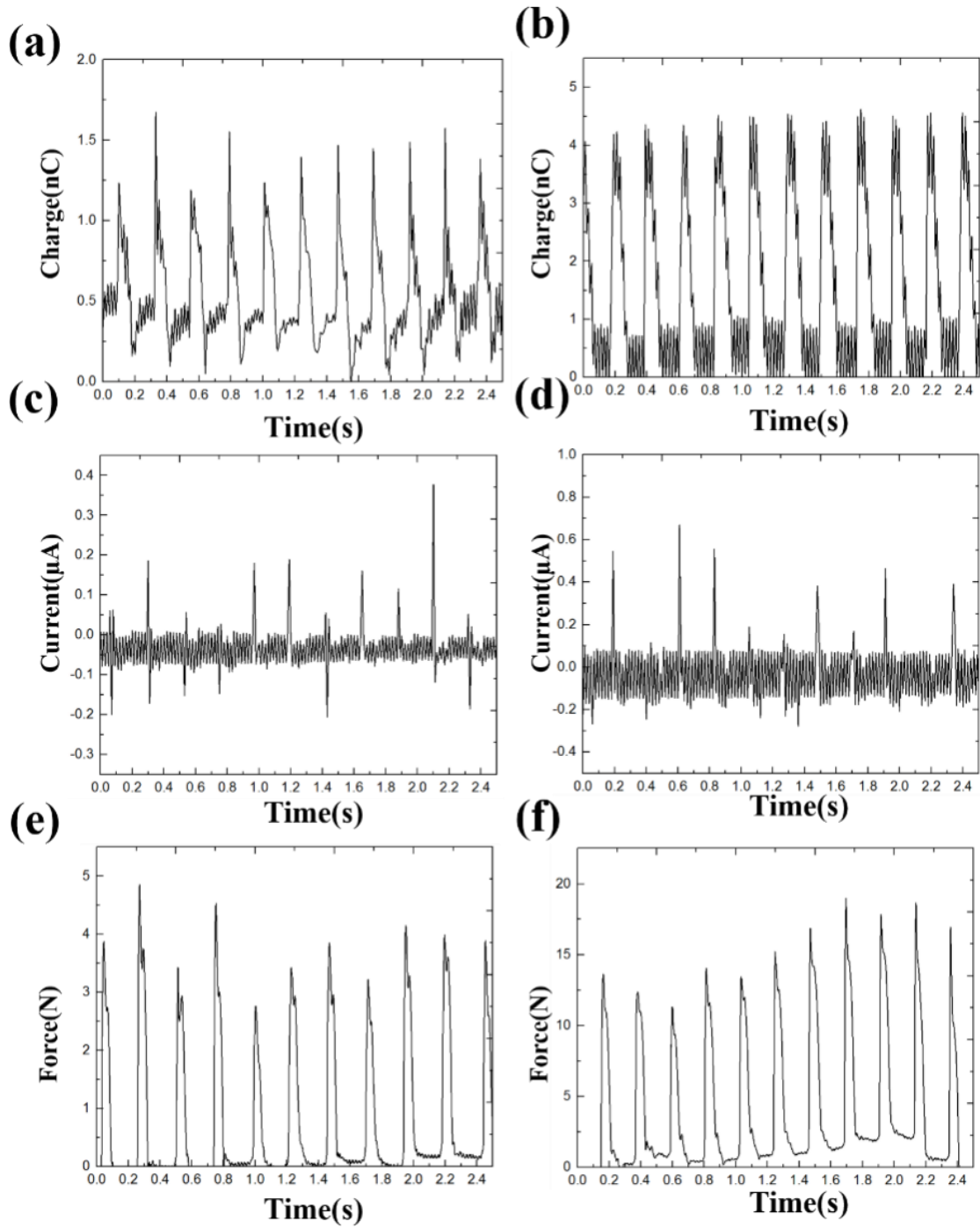


Figure S 6. Input signal of WATENG for neural branch stimulation. Output charge by applying (a) small force and (b) large force, respectively; Output current by applying (c) small force and (d) large force, respectively; Force measurement for (e) small force and (f) large force, respectively.

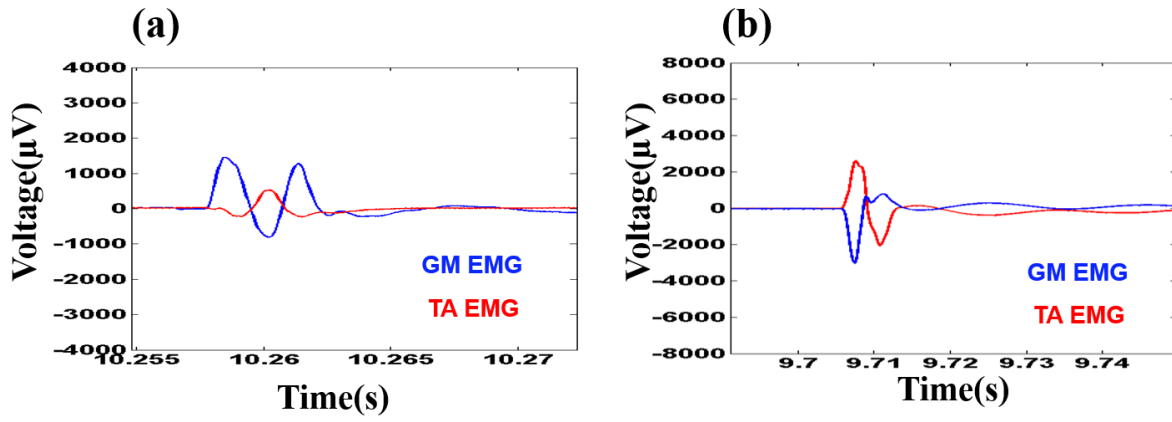


Figure S 7. The recorded compound muscle action potentials (CMAPs) from (a) the tibial nerve and (b) the CP nerve when small force was applied, respectively.

Section S8. Force recording system

A force gauge (Vernier Software & Technology) was connected to the leg of the rat with a wire. When the nerve was electrically stimulated, the leg kicked forward and thus pulling the force gauge through the wire. The force gauge was connected to a DAQ (National Instruments), and the DAQ was connected to a laptop. On the laptop, Labview (National Instruments) was used for data display. Continuous force data was recorded, and analyzed with Matlab after the experiment.

Reference

- [1] Moon, J.K., Jeong, J., Lee, D. and Pak, H.K., *Nat. Commun.* 4 (2013) 1487.
- [2] Kwon, S.H., Park, J., Kim, W.K., Yang, Y., Lee, E., Han, C.J., Park, S.Y., Lee, J. and Kim, Y.S., *Energy & Environmental Science*, 7 (2014) 3279-3283.
- [3] Helseth, L.E. and Guo, X.D., *Smart Materials and Structures*, 25 (2016) p.045007.
- [4] Helseth, L.E., *Journal of Electrostatics*, 81 (2016) 64-70.
- [5] Kim, D. and Yun, K.S., 2015. Energy harvester using contact-electrification of magnetic fluid droplets under oscillating magnetic field. In *Journal of Physics: Conference Series*, 660 (2015) 012108.
- [6] T. J. Tim Boretius, Christian Koehler, Sven Kerzenmacher, Harald Hillebrecht, Thomas Stieglitz, *IEEE EMBS*, (2011) 5404-5407.
- [7] Y. F. Rui, J. Q. Liu, B. Yang, K. Y. Li, and C. S. Yang, *Biomed Microdevices*, 14 (2012) 367-373.
- [8] C. Zhang et al., *Microsystem Technologies*, 21 (2013) 139-145.
- [9] W. Franks, I. Schenker, P. Schmutz, and A. Hierlemann, *IEEE Trans Biomed Eng*, 52 (2005) 1295-1302.
- [10] H. Yu, W. Xiong, H. Zhang, W. Wang, and Z. Li, *Journal of Microelectromechanical Systems*, 23 (2014) 1025-1035.
- [11] H. K. Naser Pour Aryan, Albrecht Rothermel, *Stimulation and Recording Electrodes for Neural Prostheses*. Springer, 2015.
- [12] M. A. Schiefer, M. Freeberg, G. J. Pinault, J. Anderson, H. Hoyen, D. J. Tyler, et al., *J Neural Eng* 10 (2013) 056006.
- [13] S. F. Cogan, *Annu Rev Biomed Eng*, 10 (2008) 275-309.